EFFECT OF A BN INTERPHASE THAT DEBONDS BETWEEN THE INTERPHASE AND THE MATRIX IN SiC/SiC COMPOSITES

Gregory N. Morscher*
Ohio Aerospace Institue; Cleveland, OH

Hee Mann Yun*
Cleveland State University; Cleveland, OH

James A. DiCarlo
NASA Glenn Research Center; Cleveland, OH

Linus Thomas-Ogbuji*
QSS Group, Inc.; Cleveland, OH

ABSTRACT

Typically, the debonding and sliding interface enabling fiber pullout for silicon-carbide fiber-reinforced silicon-carbide matrix composites with BN-based interphases occurs between the fiber and the interphase. Recently, composites have been fabricated where interface debonding and sliding occurs between the BN interphase and the matrix. This results in two major improvements in mechanical properties. First, significantly higher failure strains were attained due to the lower interfacial shear strength with no real loss in ultimate strength properties of the composites. Second, significantly longer stress-rupture times at higher stresses were observed in air at 815°C. In addition, no real loss in mechanical properties was observed for composites that did not possess a thin carbon layer between the fiber and the interphase when subjected to burner-rig exposure. Outside debonding is hypothesized to be due to two primary factors: a weaker interface at the BN/matrix interface than the fiber/BN interface and a residual tensile/shear stress-state at the interface of melt-infiltrated composites. Also, the occurrence of outside debonding was believed to occur during composite fabrication, i.e., on cool down after molten silicon infiltration.

INTRODUCTION

For woven SiC/SiC composites with BN interphases, the typical interface where debonding and sliding occurs is between the fiber and the BN interphase. We refer to this phenomenon as "inside debonding". Unfortunately, the inside debonding of the interphase

* Senior Research Scientist residing at NASA Glenn Research Center, Cleveland, OH

exacerbates the environmental durability problem of SiC/SiC composites with BN interphases at intermediate temperatures (600 to 1000°C) in the presence of oxidizing atmospheres [1,2]. When matrix cracks are formed, the environment has direct access to the fibers themselves. This causes oxidation of the BN interphase preferentially at both the fiber/BN and BN/CVI SiC interfaces as well as oxidation of the fiber surface (Figure 1a). The liquid boria reaction product reacts with the SiC fiber to form a borosilicate liquid that increases in SiO_2 content with further oxidation of the SiC. Also, B_2O_3 reacts with water vapor in the atmosphere to form volatile B-containing hydrated species resulting in an even higher SiO_2 content in the oxidation product. These phenomena result in a solid oxidation product (glass) that strongly bonds fibers bridging the matrix crack to one another or to the matrix itself and causes subsequent composite embrittlement (Figure 1a).

One proposal to curtail this type of rapid oxidative process that leads to composite embrittlement would be for the debonding and sliding interface to be some distance away from the reinforcing fibers [3]. For SiC/SiC composites this has been attempted with C/SiC multilayers as the "interphase" [3-5] and more recently with BN/SiC multilayers [6]. In theory, debonding and sliding would occur in some of the outer layers, prohibiting or complicating the diffusion of oxidizing species to the inner fiber/interphase region that leads to composite embrittlement. Some benefit has been demonstrated for stress-rupture of minicomposites with multilayer C/SiC coatings [7,8].

For SiC/SiC composites with BN interphases, if the debonding and sliding layer was between the BN and the matrix, a similar benefit proposed for the multilayer approach could be achieved. Oxidation of the BN would occur from the "outside" of the BN inwards toward the fiber. The resulting boria oxidation product would react with the SiC matrix to eventually form a borosilicate glass that would act as a "sealant" slowing diffusion of oxidizing species to the BN. In order for the fibers to be fused together or to the matrix, oxidation of the entire thickness of the BN would have to occur (Figure 1b). This may take a considerable amount of time considering the effects of sealing and the reduced surface area of BN exposed to oxidizing species when compared to the typical "inside" debonding case (Figure 1a and b). Therefore, the major benefit expected from an outside debonded interphase in SiC/SiC composites would be improved intermediate temperature mechanical properties, e.g., stress-rupture, in oxidizing

environments. Such behavior has been demonstrated and will be described and discussed in this work.

EXPERIMENTAL

SiC fiber reinforced melt-infiltrated SiC matrix composite panels that exhibited outside debonding were fabricated from 2D-woven, balanced, 5 harness satin, 0/90 fabric, by General Electric Power Systems Composites (Newark DE). The composite fabrication process involves the following steps: chemical vapor infiltration (CVI) of a stacked (~ 152 mm x 229 mm) 2D woven fabric with BN, CVI SiC infiltration, SiC particle slurry infiltration, and final liquid Si infiltration [9]. The occurrence of outside debonding was initially a processing aberration, but has since been under study in order to optimize and control its occurrence. Outside debonding was observed for over 20 different SiC/SiC composite panels fabricated with Sylramic® (Dow Corning, Midland, MI) fibers, Hi-Nicalon Type S (Nippon Carbon, Tokyo Japan), and Sylramic-iBN (treated Sylramic® fibers that possess an in-situ BN coating [10]). Most of the panels were fabricated with Sylramic-iBN or Sylramic® fibers and ranged in fiber volume fraction in the loading direction from 0.13 to 0.25. Table I lists some of the variations in the physical characteristics of composite panels.

Mechanical property evaluation included room and intermediate temperature tensile testing. Room temperature tensile testing was performed on at least two dogbone specimens from each panel. Dogbone specimens were cut so that the gage section was 10 mm wide and the grip section was 12.5 mm wide. Both monotonic and load/unload/reload hysteresis tensile tests were performed while being monitored by modal acoustic emission (AE) [11]. Intermediate temperature stress-rupture tests were performed in air at 815°C as in reference 3. Specimens from some panels were also subjected to an atmospheric pressure burner-rig under zero-stress exposure at 815°C, i.e., uncracked, and then tensile tested at room temperature in order to determine the retained strength [12].

Fracture surfaces of the failed composites were examined with a Field Emission Scanning Electron Microscope (FESEM), Hitachi model S-4700. A fiber push-in technique [13,14] was performed on polished sections of untested panels to determine the interfacial shear stress of the sliding interface. At least twenty different fibers were tested for each specimen. Finally, the interphase region of some specimens was examined using Auger Electron Spectroscopy (AES)

and Transmission Electron Microscopy (TEM). For AES, small slivers of composite material were fractured in bending in-situ under vacuum in order to prevent the fracture surface from contamination. Depth profiles were then performed at regions where the BN layer adhered to the matrix and at other regions where the BN layer adhered to the fiber.

RESULTS

Room Temperature Tensile Stress-Strain Behavior

Typical monotonic and unload-reload tensile hysteresis stress-strain curves are shown in Figure 2 for MI SYL-iBN/SiC composite that displays inside and outside debonding. Acoustic emission was monitored for both and is plotted in the strain-domain as well as stress-domain (insets in Figure 2). It was observed that the first detectable AE that occurs in the gage section occurs at 110 +/- 20 MPa for both inside and outside debonding composites. This is typical for all 2D woven SiC fiber reinforced MI matrix composites [15]. Also note that upon unloading the material stiffens indicating that the matrix is in residual compression. A measure of the residual stress can be approximated from the intersection of the average slopes of the hysteresis loops for stresses higher than approximately half the peak stress of the hysteresis loop (Figure 2) [16].

Figure 3 shows typical stress-strain curves (hysteresis loops removed) for the same architecture MI composites with "outside" and "inside" debonding. In general, although similar in ultimate strength, two differences between outside and inside debonding composites were evident for room temperature stress-strain behavior: "outside debonding" composites had (1) lower elastic moduli (Table I) and (2) a higher strain at a given applied stress including higher strains to failure (Table I and Figure 3). However, one panel, which exhibited a mixture of inside and outside debonding, was an exception and had a high elastic modulus (246 GPa).

Figure 4 shows examples of composite fracture surfaces after room temperature tensile failure. Some bundle pull-out was observed for both types of composites; however, individual fiber pull-out was significantly longer for outside debonding composites (Figures 4a and b) than for inside debonding composites (Figures 4c and d). Note the adherence of the BN layer to the fibers for the outside debonding composites (Figure 4b). It would be ideal if debonding outside the BN interphase occurred for each fiber independently from one another (e.g., Figure 1). However, due to the close packing of fibers in woven bundles, debonding between the BN-interphase and the matrix was often observed to occur around groups of fibers that were linked to

one another by the thin BN that was deposited on two closely spaced fibers. Usually, these fiber groups were made up of a few fibers that formed a row of fibers rather than a "ring" of fibers as shown in Figure 4b. Debonding at the BN-interphase/SiC matrix was observed for individual fibers that were well separated from other fibers, i.e., a SiC matrix separated the BN interphase around two fibers, and often fibers that were separated only by the BN interphase were observed to detach from one another so that BN stayed adhered to both fibers. There of course were observations of BN only adhering to one fiber, leaving the neighboring fiber surface bare. For some composites, regions of outside debonding and inside debonding were observed in different regions or bundles of the fracture surface, i.e., mixed debonding. It should also be noted that debonding sometimes occurred around entire bundles of tightly packed fibers, but this occurs for both outside and inside debonding composites (Figure 4a and c).

In addition to a low elastic modulus, outside debonding composites often displayed a secondary modulus prior to significant matrix cracking. Figure 5 shows a family of stress-strain curves for a number of different outside debonding composites with different fiber architectures and volume fractions. The initial elastic moduli were very consistent (~ 218 GPa) and all of the curves showed an inflection at ~ 70 MPa that resulted in a lower secondary modulus (~ 177 MPa). This inflection was not associated with any AE activity, i.e., it appears that this inflection was not due to matrix crack formation.

Finally, the interfacial shear strength of several different inside debonding and outside debonding composites was determined using two techniques [14]. First, the interfacial shear strength was estimated by modeling the stress-strain curve based on the stress-dependent crack density (from AE). Composite strain was determined in the same fashion as Pryce and Smith [17]. Using the nomenclature of Curtin, et al. [18], composite strain can be modeled assuming equally spaced cracks:

$$\varepsilon = \sigma/E_c + \alpha\delta(\sigma)\rho_c/E_f\ (\sigma + \sigma_{th}); \qquad \text{for } \rho_c^{-1} > 2\delta \tag{1}$$

where σ is the applied stress, σ_{th} is the residual (thermal) stress in the matrix (compression is negative), E is the elastic modulus, subscripts m, f and c refer to matrix, fiber, and composite, respectively, ρ_c is the matrix crack density. The first part of the equation corresponds to the elastic strain response of an uncracked composite and the second part of the equation

corresponds to the extra strain (displacement) of the fibers at and away from a through-thickness matrix crack dictated by the sliding length:

$$\delta = \alpha\, r\, (\sigma + \sigma_{th}) / 2\tau \quad (2)$$

where

$$\alpha = (1\text{-}f)\, E_m / f\, E_c \quad (3)$$

and r is the fiber radius, f is the fiber volume fraction in the loading direction, and τ is the interfacial shear strength. E_c and σ_{th} were determined from the stress strain curves. E_f is 380 GPa and E_m was determined from the rule-of-mixtures. The stress dependent ρ_c was estimated from the measured final crack density of failed composites multiplied by the normalized cumulative AE energy (Figure 2), assuming the latter represented the stress-dependent distribution of matrix cracks, which has been demonstrated for similar systems [11, 19]. Therefore, the only variable not known was τ which was adjusted in order to best fit the predicted stress strain curve to the experimental stress strain curve. For the case where the sliding lengths overlap, Ahn and Curtin [20] showed that if the cracks are still equally spaced, the composite strain could then be modeled by:

$$\varepsilon = \sigma / (f E_f) + \alpha\, \sigma_{th} / E_f - \alpha\, (\sigma + \sigma_{th}) / [4\, E_f\, \delta(\sigma)\, \rho_c]; \text{ for } \rho_c^{-1} < 2\delta \quad (4)$$

Therefore, for higher applied stress conditions, if $\rho_c^{-1} < 2\delta$ was predicted, equation (4) was used. Figure 6 shows an example of a best-fit stress-strain curve for an inside debonding composite specimen.

The interfacial shear stress was also measured directly from the fiber push-in technique. Results of the two techniques are listed for individual specimens in Table I for systems which displayed global outside debonding, mixed outside/inside debonding, and global inside debonding. Both techniques confirmed that the interfacial shear strength of global outside debonding composites (~ 10 MPa) was significantly less than that of inside debonding composites (~ 70 MPa). Mixed outside/inside debonding had intermediate values of interfacial shear strength. It is important to note that even though the interfacial shear strength of outside debonding is lower than that of inside debonding composites, there was no loss in ultimate strengths for outside debonding composites and often the ultimate strength increased (e.g. compare the f = 0.2 composites in Figure 3a).

Intermediate Temperature Mechanical Behavior

Stress rupture at 815°C was performed on SYL and SYL-iBN composites with inside and outside debonding (Figure 7). The stresss-rupture data for SYL SiC/SiC composites displaying inside debonding have been reported in references 21 and 22. Since the panels varied in fiber volume fraction, the rupture stress data is plotted as the stress on the fibers, i.e., the load in a matrix crack that was carried by the fibers. For comparison, the rupture stress corresponding to a composite with f = 0.2 in the loading direction is shown on the right axis. Each set of data for the different types of composites had at least one panel with f = 0.2.

First, note that there is a difference in rupture behavior between inside debonding SYL-iBN fiber composites and SYL fiber composites. Inside debonding SYL-iBN composites outperform (i.e., fail after a longer time at a given stress) inside debonding SYL composites because the fibers in SYL-iBN composites are naturally spread apart from one another with the formation of the ~ 100nm BN layer on the fiber surface [22]. The rupture life depends on the time it takes to bond nearest-neighbor fibers together, which takes more time with increasing separation distance. In addition, the debonding interface for inside debonding SYL-iBN actually occurs between the in-situ BN and the CVI deposited BN [10]. In other words, for inside debonding SYL-iBN composites, the debonding and sliding interface was some distance (~ 100 nm) away from the fiber surface, which contained SiC.

For both fiber composite systems possessing an outside debonding interface, further improvements in intermediate temperature stress-rupture life were observed (Figure 7). For SYL composites with outside debonding compared to SYL inside debonding composites, stress-rupture improved by over 250 MPa in fiber stress (~ 50 MPa for a f=0.2 composite). For outside debonding SYL-iBN composites in comparison to inside debonding SYL-BN composites, there was over an order of magnitude in time improvement at high stresses and ~ 200 MPa improvement in fiber stress (~ 40 MPa for a f=0.2 composite) at lower stresses near the run-out condition. It should be noted that these high stress conditions for stress-rupture are significantly higher than the stresses for matrix cracks to penetrate the load-bearing fibers (determined from the onset of hysteresis loop activity, ~ 175 MPa for f=0.2 composites used in this study). In other words, the SYL-iBN composites are significantly cracked at the stress-rupture conditions of this study, even for specimens that did not fail after long periods of time.

Examination of the rupture specimen fracture surfaces confirmed the survival of most of the BN around the fibers in the matrix crack even though significant oxidation had occurred in the matrix crack (Figure 8). However, at regions of near fiber-to-fiber contact, the thinner areas of BN were oxidized and fiber-to-fiber fusion occurred for rupture times greater than 80 hours. There were a several regions of significant fiber pullout throughout the cross-section of the fracture surface.

It was observed for inside debonding composites with Hi-Nicalon^{TM} (Nippon Carbon, Japan) fibers that a composite specimen with an increased number of cracks, e.g., a specimen precracked at a higher stress than the rupture condition, had shorter rupture lives when tested at the same stress as a pristine specimen [22]. This was attributed to the mechanism of composite embrittlement: the failure of a fiber that is strongly bonded to another fiber which creates a catastrophic unbridged matrix crack to propagate through the rest of the strongly bonded fibers in the matrix crack. If more cracks exist, due to the statistical nature of fiber failure, it is more likely that a bridged fiber that is strongly bonded will fail at a shorter time because a longer effective length of fibers are bridging the matrix cracks. This was demonstrated and modeled in reference 22. With that in view, in this study, a few specimens (SYL and SYL-iBN) were precracked at room temperature and compared to the rupture behavior of pristine specimens from the same panel (Figure 9).

Unfortunately only a few specimens were available, but it is evident that inside debonding SYL composites with nominally good rupture properties were significantly poorer in rupture behavior with precracking. On the other hand, the outside debonding specimen with SYL-iBN fibers that was precracked did not fail after 330 hours compared to the pristine specimen which failed after ~ 190 hours. With such little data it is not possible to conclude that precracked outside debonding specimens are superior to pristine specimens in rupture; however, this does demonstrate that the rupture properties of outside debonding composites are at least unaffected by the damage state.

Sylramic, SYL-iBN, and HNS outside debonding composites were subjected to burner rig exposure at 815°C for ~ 100 hour with no applied stress, and then were tested at room temperature to determine the retained strength properties. Whereas the rupture tests evaluate the durability of composites when cracked, the zero-stress burner rig experiment has proven to be an effective test to evaluate the ability of an undamaged composite material to withstand severe

intermediate temperature oxidation through the exposed (as-machined) edges of the composite specimen. It has been found that if carbon exists on the surface of any fiber-type, the SiC/SiC MI composites will be significantly degraded after burner rig exposure. This type of degradation has been observed for (1) Hi-Nicalon due to a carbon-rich layer that occurs for MI composites after fiber and composite processing [12], (2) Hi-Nicalon S^{TM} due to a carbon rich layer on the fiber surface after fiber processing [23], and (3) Sylramic® composites when a sizing is used on the fibers that was not burned off completely prior to BN interphase deposition [24]. SYL and SYL-iBN composites with a sizing that has low char yield are unaffected by burner-rig exposure. Figure 10 compares the burner rig degradation (or lack thereof). Also shown is an example of outside debonding SYL-iBN before and after burner-rig exposure. No significant strength degradation has been observed for SYL-iBN and SYL composites with outside debonding and complete sizing removal. Burner-rig exposed SYL-iBN and Sylramic composites with outside debonding were often observed to stiffen and fracture at slightly lower ultimate strain (Figure 10, Sylramic composite not shown). However, HNS outside debonding composites were degraded after burner-rig exposure due to the presence of a carbon layer on the fiber surface. HNS outside debonding composites were also observed to stiffen slightly after burner-rig exposure. Stiffening does not occur for inside debonding composites.

Some fracture surfaces were examined from burner-rig exposed SYL and SYL-iBN composites. The composites exhibited long pull-out lengths similar to as-produced specimens (Figure 4a) and a SiO_2 containing layer was often observed on the surface of the BN in between the BN and the matrix throughout the cross-section (Figure 11). Evidently, oxidation occurred through the BN/CVI SiC interface region at the exposed cut edge into the interior of the composite. HNS composites exhibited a flat fracture surface and strong bonding of fibers as has been reported for other systems with carbon layers that exist at the fiber surface [24].

Analysis of the BN-CVI SiC Interface

AES depth profiles were carried out on specimen surfaces that were fractured in the AES chamber for several specimens exhibiting inside and outside debonding. Depth profiles through BN layers adhered to the CVI SiC matrix are shown in Figure 12 for representative specimens. A mild enrichment of C appears to exist at the BN-CVI SiC interface for both inside and outside debonding specimens. There may be a slightly higher proportion of C enrichment for specimens

that exhibit outside debonding. However, the difference in the amount of C enrichment between inside and outside debonding composites was not very much and given the error in the AES measurement (~ 10%) cannot be considered conclusive.

Representative TEM micrographs of inside and outside debonding specimens are shown in Figure 13. Also shown are C maps of the same region. There does appear to be some C enrichment at the BN-CVI SiC interface for the outside debonding composites and little if any C enrichment for the inside debonding composites.

DISCUSSION

Improved Mechanical Properties

The increased strain to failure of outside debonding composites can be attributed to the lower τ of the BN-CVI SiC interface over that of the fiber/BN interface. However, if τ decreased and global load sharing exists, one would expect the ultimate strength properties to decrease [25]. The converse has been observed for strongly bonded interfaces compared to weakly bonded interfaces in CVI SiC matrix composites where the higher τ interface composites exhibit higher ultimate strengths [26]. In this study, the lower τ composites did not lose strength and in some cases were stronger than comparable high τ composites. Two explanations can account for this. First, it is possible that high τ composites exhibit local load sharing and the lower τ composites exhibit global load sharing. If the high τ composites exhibit local load sharing, stress-concentrations would develop for load-bearing fibers surrounding individual or groups of broken fibers in a matrix crack. This would result in lower composite ultimate strengths than expected based on global load sharing [27]. Second, global load sharing may occur for both low and high τ composites and as Xia and Curtin [28] have theorized, fibers with an adhered coating would be effectively stronger than fibers without a coating because the flaws on the fiber surface are constrained to some degree by the coating, even for low modulus coatings such as C or BN. In fact, their model would predict approximately the same composite strength for outside debonding composites with a τ = 10 MPa and inside debonding composites with a τ = 70 MPa.

The improved intermediate temperature rupture life of outside debonding composites occurs in the manner put forward in Figure 1b (Figure 8). Even after 100 hours at 815°C in a bridged matrix crack, a significant portion of the BN remained as a barrier between the oxidation

reaction product and the fiber surface for the majority of fiber circumference. However, thinner regions of BN separating nearest neighbor fibers were oxidized and appear to have led to the time-dependent strength degradation. This would explain why the Sylramic® composites with outside debonding are poorer in stress-rupture than the Sylramic-iBN composites (Figure 8). The former consists of many fibers nearly contacting another fiber with little or no BN interphase in between, whereas the latter possesses the in-situ BN layers on the fiber surface that enable greater protection of the fibers as well as some degree of fiber-separation. Finally, for typical inside debonding composites that fail at significantly shorter lives and lower stresses at the same temperature, no BN was detectable in the oxidized portion of a fracture surface (see e.g. references 1 and 29). In other words, the entire matrix and interphase region of inside debonding composites would be completely oxidized, with the fibers strongly bonded to the matrix.

Why outside debonding?

Two potential mechanisms are considered for outside debonding for these MI composite systems: (1) a weaker BN-CVI SiC interface than BN-fiber interface and (2) sufficient residual stress at the interface to cause debonding of the weak interface probably on cooling after infiltration of molten Si. The outside debonding composites possess a lower τ than inside debonding composites (Table I), presumably, the debond energy of the BN/CVI-SiC interface is also lower than the debond energy of the fiber/BN interface as well. Residual compression exists in the matrix (Figure 2), which presumably forces the fibers into residual tension. This is due to free Si. The volume expansion of Si from the liquid to solid state is ~ 9%. Therefore, expansion of the Si phase takes place during cooling of the composite from its fabrication temperature for MI (~ 1400°C depending on the additives to the Si). This places the Si in compression. Si also has a lower thermal expansion coefficient than SiC, ~ 3 x 10^{-6} /°C compared to ~ 4.5 x 10^{-6} /°C, respectively. Therefore, upon further cooling, the Si is placed in further compression. The crack closure effect (Figure 2) reflects the global residual stress state of the entire matrix, i.e., the free Si, the particulate SiC, the CVI SiC, and the unbridged 90° fiber/interphase bundles taken together are in residual compression necessitating residual tension in the fibers. Locally, the residual stress states would be expected to be quite complex. Nevertheless, the interphase and interfaces between the fibers and matrix, should be subjected to residual tensile and shear stress. This could create the scenario where, if the strength of those interfaces were weak enough, the

interface could debond during cooling of the composite or result in a stress-state ahead of an approaching crack that could lead to preferential debonding of the BN-CVI SiC interface rather than the fiber-BN interface. In this regard, since MI systems will inherently have residual compression in the matrix, they may be an ideal composite system to enable outside debonding. Although, outside debonding type of behavior has been observed in SiC/BN/CVI SiC minicomposites with tailored BN interfaces [30].

The proposition that the interface debonded on cooling has experimental merit based on the room temperature stress-strain properties. Outside debonding composites had lower elastic moduli and the occurrence of a "secondary modulus" at low stress (Figure 5). Debonding of fibers and tows would be expected to lower the modulus in the same manner as porosity. It is interesting to note that the measured residual stress in outside debonding composites was found to be often, but not always, lower than that of similar architecture composites [14] when using the approach of Steen [16]. This could be due to the relief of some of the residual stress in the composite with interface debonding during cooling. The observance of a "secondary modulus" not associated with matrix cracking may be indicative of the actual stiffness of the already debonded composite. When the composite reaches a certain tensile stress, the residual compressive stress-state that exists in the matrix, which would include the net effect of the 90° bundles, would be overcome. This would be similar to the crack-closure phenomenon that occurs for SiC fiber-MI composites at stresses high enough to cause unload-reload hysteresis loops where the unloading curve stiffens at low stresses due to crack closure, i.e. compression in the matrix (Figure 2). For the case of outside debonding, the matrix would effectively be microcracked at the already debonded BN-CVI SiC interface.

Regarding the observance of a weaker BN-matrix interface for outside debonding CMCs, the presence of carbon either as a thin layer outside of the BN or in an enriched form appears to be the most likely factor, even though the detection of carbon enrichment is not compelling. One other possible explanation is that differences in processing conditions led to more shrinkage of the low temperature deposited BN. BN shrinkage, the formation of a gap between the BN and the CVI SiC, and outside debonding has been observed for fiber/BN/CVI SiC preforms that have been heat treated to higher temperatures [31]. Nevertheless, oxidation that occurs between the BN and the CVI-SiC matrix during burner rig exposure clearly implies either the presence of a C layer, as was the case for the earlier mentioned composite systems where a thin C layer existed

between the fiber and the BN [15,23-24], or the existence of a "gap" between the BN and the CVI-SiC, i.e., an already debonded interface prior to testing.

Issues to be Resolved

Finally, even though outside debonding composites offer potential improvements in stress-strain and intermediate temperature properties, further study is still required to address other pertinent composite properties. Most notably are the effects of outside debonding on through-thickness properties: interlaminar tensile strength, interlaminar shear strength, and through-the-thickness thermal conductivity. Another issue is the ability to reproducibly control outside debonding behavior. All of these issues are currently being studied and some modifications may have to be made to optimize composite properties for a given application. It should be noted that the tensile creep at elevated temperatures (up to 1315°C in air) of outside debonding composites in the fiber direction were as good as inside debonding composites [32].

CONCLUSION

MI SiC/SiC composites with BN interphases that exhibited interface debonding and sliding at the BN-CVI SiC interface showed significantly higher strain capabilities and intermediate temperature stress-rupture life over conventional composites that exhibit interface debonding and sliding at the BN-fiber interface. Higher strain to failure was attributed to lower interfacial shear stress at the BN-CVI SiC interface. Improved intermediate temperature properties were attributed to the protection from the oxidizing environment due to the adherence of the BN layer to the fiber surface, which is not the situation for the inside debonding composites. Thus the environment does not have direct access to the fibers, which prohibits or stalls the rapid strength-degrading oxidative process of strongly bonding fibers to nearest neighbor fibers. In addition, no degradation in retained strength was observed after burner rig exposure, which typically occurs when carbon exists at the fiber/BN interface.

The cause of outside debonding was believed to be due to (1) a weaker BN/CVI-SiC interface than BN/fiber interface, perhaps caused by the presence of C at the BN/CVI-SiC interface, and (2) residual tensile/shear stress at the BN-CVI SiC interface that was sufficient to cause interface debonding during cool-down after composite processing. The residual stress-state in SiC fiber/MI composites is primarily caused by the infiltration of molten Si in the final

step of matrix processing. The volume expansion of the Si liquid to solid phase transformation coupled with a lower thermal expansion coefficient for Si compared to SiC results in residual compression in the matrix of SiC fiber/MI matrix composites. For this reason, outside debonding is expected to be easier to tailor for MI composites compared to other SiC fiber, SiC matrix combinations.

REFERENCES:

1. G.N. Morscher, J. Hurst, and D. Brewer, "Intermediate-Temperature Stress Rupture of a Woven Hi-Nicalon, BN-Interphase, SiC-Matrix Composite in Air," *J. Am. Ceram. Soc.*, **83** [6] 1441-49 (2000)
2. N.S. Jacobson, G.N. Morscher, D.R. Bryant, and R.E. Tressler, "High-Temperature Oxidation of Boron Nitride: II, Boron Nitride Layers in Composites," *J. Am. Ceram. Soc.*, **82** [6] 1473-82 (1999)
3. H. W. Carpenter and J. W. Bohlen, "Fiber Coatings for Ceramic Matrix Composites," *Ceram. Eng. Sci. Proc.*, **13** [7-8] 23-56 (1992).
4. R. Naslain, "The Concept of Layered Interphases in SiC/SiC"; pp. 23-39 in High-Temperature Ceramic-Matrix Composites II. Edited by A. G. Evans and R. Naslain. American Ceramic Society, Westerville, OH, 1995.
5. F. Rebillat, J. Lamon, R. Naslain, E. Lara-Curzio, M. K. Ferber, and T. M. Besmann, "Properties of Multilayered Interphases in SiC/SiC Chemical-Vapor-Infiltrated Composites with 'Weak' and 'Strong' Interfaces," *J. Am. Ceram. Soc.*, **81** [9] 2315-26 (1998).
6. S. Betrand, O. Boisron, R. Pailler, J. Lamon, and R. Naslain, "(PyC/SiC)n and (BN/SiC)n Nanoscale-Multilayered Interphases by Pressure-Pulsed CVI," in Key Engineering Materials, Vols. 164-165, 1999, Trans. Tech Publications, Switzerland., pp. 164-165.
7. Pasquier, S., Lamon, J., and Naslain, R., Static fatigue of 2D SiC/SiC composites with multilayered (PyC-SiC)n interphases at high temperatures in air. in Key Engineering Materials, Vols. 164-165, 1999, Trans. Tech Publications, Switzerland., pp. 249-252.
8. S. Bertrand, R. Pailler, and J. Lamon, "Influence of Strong Fiber/Coating Interfaces on the Mechanical Behavior and Lifetime of Hi-Nicalon/(PyC/SiC)n/SiC Minicomposites," *J. Am. Ceram. Soc.*, **84** [4] 787-94 (2001)

9. D. Brewer, "HSR/EPM Combustor Materials Development Program" *Mater. Sci. Eng. A*, **A261**, 284-291 (1999).
10. H.M. Yun and J.A. DiCarlo, "Comparison of the Tensile, Creep, and Rupture Strength Properties of Stoichiometric SiC Fibers," *Cer. Eng. Sci. Proc.*, **20** [3] 259-272 (1999)
11. G.N. Morscher, "Modal Acoustic Emission of Damage Accumulation in a Woven SiC/SiC Composite," *Comp. Sci. Tech.* **59** 687-697 (1999).
12. L.U.J.T. Ogbuji, "A Pervasive Mode of Oxidation Degradation in a SiC-SiC Composite," *J. Am. Ceram.*, **81** [11] 2777 (1998)
13. J.I. Eldridge, "Desktop Fiber Push-Out Apparatus," NASA Technical Memorandum 105341, December 1991.
14. G.N. Morscher and J.I. Eldridge, "Constituent Effects on the Stress-Strain Behavior of Woven Melt-Infiltrated SiC Composites," ICF 10 in print
15. G.N. Morscher, J.Z. Gyekenyesi, and R.T. Bhatt, "Damage Accumulation in Woven SiC/SiC Composites," *Environmental, Mechanical, and Thermal Properties and Performance of Continuous Fiber Ceramic Composite (CFCC) Materials and Components, ASTM STP 1392,* M.G. Jenkins, Ed., American Society for Testing and Materials, West Conshohocken, PA, 2000. pp. 306-319.
16. M. Steen and J.L. Valles, "Unloading-Reloading Sequences and the Analysis of Mechanical Test Results for Continuous Fiber Ceramic Composites," *ASTM STP 1309*, M. G. Jenkins et al., Ed., American Society for Testing and Materials , West Conshohocken, PA, 1997, pp. 49-65.
17. A.W. Pryce and P.A. Smith, "Matrix Cracking in Unidirectional Ceramic Matrix Composites Under Quasi-Static and Cyclic Loading," *Acta metal. mater.*, **41** [4] 1269-1281 (1993)
18. W.A. Curtin, B.K. Ahn, and N. Takeda. "Modeling Brittle and Tough Stress-Strain Behavior in Unidirectional Ceramic Matrix Composites," *Acta mater.*, **46** [10] 3409-3420 (1998)
19. G.N. Morscher, "Modal Acoustic Emission Source Determination in Silicon Carbide Matrix Composites," in Review of Progress in Quantitative Nondestructive Evaluation, eds. D.O. Thompson and D.E. Chimenti, CP 509, American Institute of Phisics, pp. 383-390 (2000)
20. B.K. Ahn and W.A. Curtin, "Strain and Hysteresis by Stochastic Matrix Cracking in Ceramic Matrix Composites," *J. Mech. Phys. Solids*, **45** [2] 177-209 (1997)

21. G.N. Morscher and J. Hurst, "Stress-Rupture and Stress-Relaxation of SiC/SiC Composites at Intermediate Temperature," *Ceram. Eng. Sci. Proc.*, **22** [3] 539-546 (2001)
22. G.N. Morscher and J.D. Cawley, "Intermediate Temperature Strength Degradation in SiC/SiC Composites," *J. European Ceramic Society*, In print.
23. H.M. Yun, J.A. DiCarlo, L.T. Ogbuji, and Y.L. Chen, "Tensile Behavior of As-Fabricated and Burner-Rig Exposed SiC/SiC Composites with Hi-Nicalon Type-S Fibers," *Ceram. Eng. Sci. Proc.*, (2002) in print
24. L.U.J.T. Ogbuji, D.R. Wheeler, and T.R. McCue, "Process-Induced Carbon Sub-Layer in SiC/BN/SiC Composites: Characterization and Consequences," *Ceram. Eng. Sci. Proc.*, **22** [3] 379-387 (2001)
25. W.A. Curtin, "Theory of Mechanical Properties of Ceramic-Matrix Composites," *J. Am. Ceram. Soc.*, **74** [11] 2837-45 (1991)
26. F. Rebillat, J. Lamon, R. Naslain, E. Lara-Curzio, M. K. Ferber, and T. M. Besmann , "Properties of Multilayered Interphases in SiC/SiC Chemical-Vapor-Infiltrated Composites with "Weak" and "Strong" Interfaces" *J. Am. Ceram. Soc.*, **81** [9] 2315-2326 (1998)
27. M. Ibnabdeljalil and W.A. Curtin, "Strength and Reliability of Fiber-Reinforced Composites: Localized Load-Sharing and Associated Size Effects," *Int. J. Solids Structures,* **34** [21] 2649-2688 (1997)
28. Z. Xia and W.A. Curtin, "Design of Fiber/Coating Systems for High Strength in Ceramic Matrix Composites," *Ceram. Eng. Sci. Proc.*, **22** [3] 371-378 (2001).
29. G.N. Morscher, H.Y. Yun, and F.I. Hurwitz, "High Temperature Si-doped BN Interphases for Woven SiC/SiC Composites," *Ceram. Eng. Sci. Proc.*, (2002) in print
30. S. Jacques, A. Lopez-Marure, C. Vincent, H. Vincent, and J. Bouix, "SiC/SiC Minicomposites with Structure-Graded BN Interphases," *J. European Ceram. Soc.*, **20** 1929-1938 (2000).
31. R. Bhatt, private communication.
32. H.Y. Yun and J. Hurst, unpublished data.

Table I: Physical and Mechanical Properties of Some of the SiC/SiC Composites Tested

Specimen – *Location of Debonding*	**epcm* / No. plies**	**f**	**E GPa**	**σ_{ult} MPa**	**ε_{ult} %**	**τ estimated from σ/ε curve MPa**	**τ measured from push-in test MPa**
HNS-Outside	*7.1/8*	*0.17*	*200*	*352*	*0.46*		--
HNS-Inside	7.1/8	0.18	240	311	0.38		--
SYL-Outside	*7.1/6*	*0.13*	*224*	*224*	*0.27*	*37*	--
SYL-Outside	*5.0/8*	*0.15*	*219*	*297*	*0.43*	*25*	--
SYL-Mixed	*7.9/8*	*0.19*	*246*	*353*	*0.33*	*45*	*26*
SYL-Inside	6.3/8	0.19	246	397	0.36	--	--
SYL-Inside	8.7/8	0.2	265	389	0.3	65	64
SYL-Inside	7.1/8	0.17	270	310	0.31	63	70
SYL-iBN Outside	*8.7/8*	*0.2*	*216*	*456*	*0.5*	*20*	*7*
SYL-iBN Outside	*7.1/8*	*0.17*	*220*	*395*	*0.49*	*11*	*6*
SYL-iBN Mixed	*7.9/8*	*0.19*	*228*	*>476*	*0.51*	*43*	*31*
SYL-iBN Inside	8.7/8	0.2	277	404	0.31	71	83
SYL-iBN Inside	7.9/8	0.2	248	502	0.42	--	--
SYL-iBN Inside	5.0/8	0.12	279	284	0.21	63	--

* tow ends per centimeter

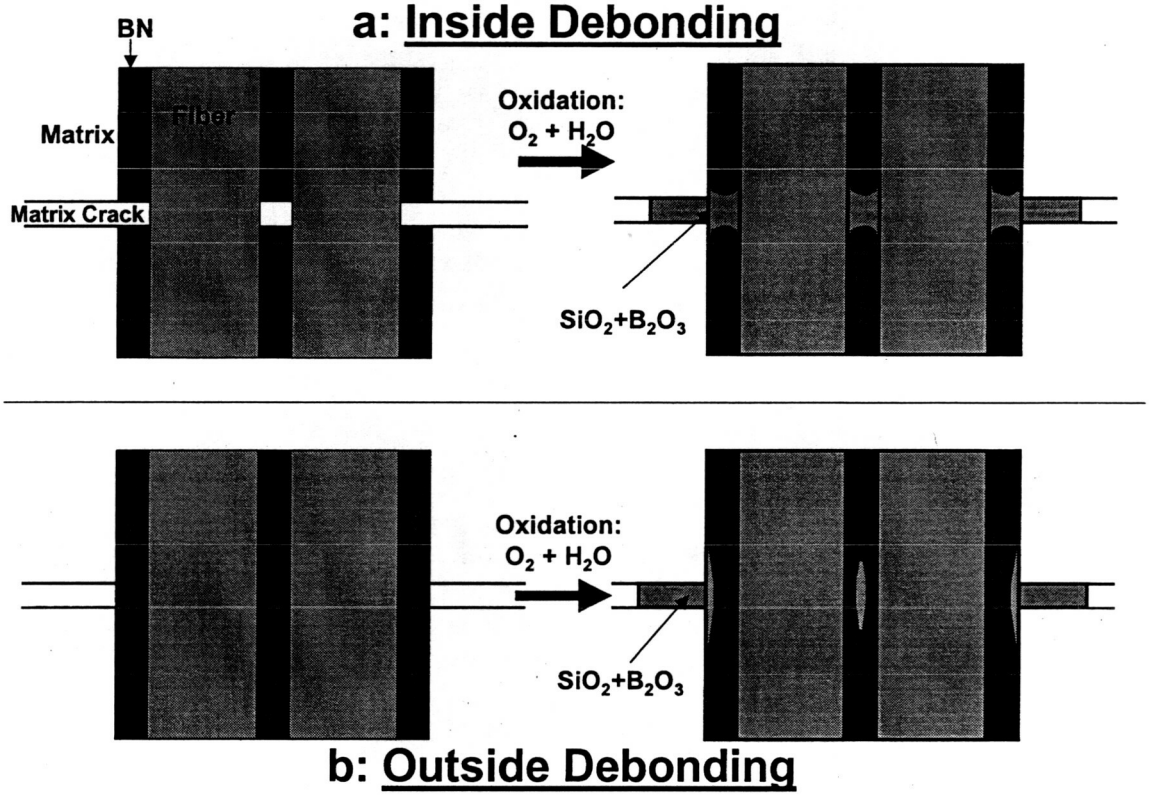

Figure 1: Schematic representation of oxidation of the interphase for (a) debonding and sliding between the fiber and the BN interphase, i.e., "inside debonding", and (b) between the BN interphase and the matrix, i.e., "outside debonding".

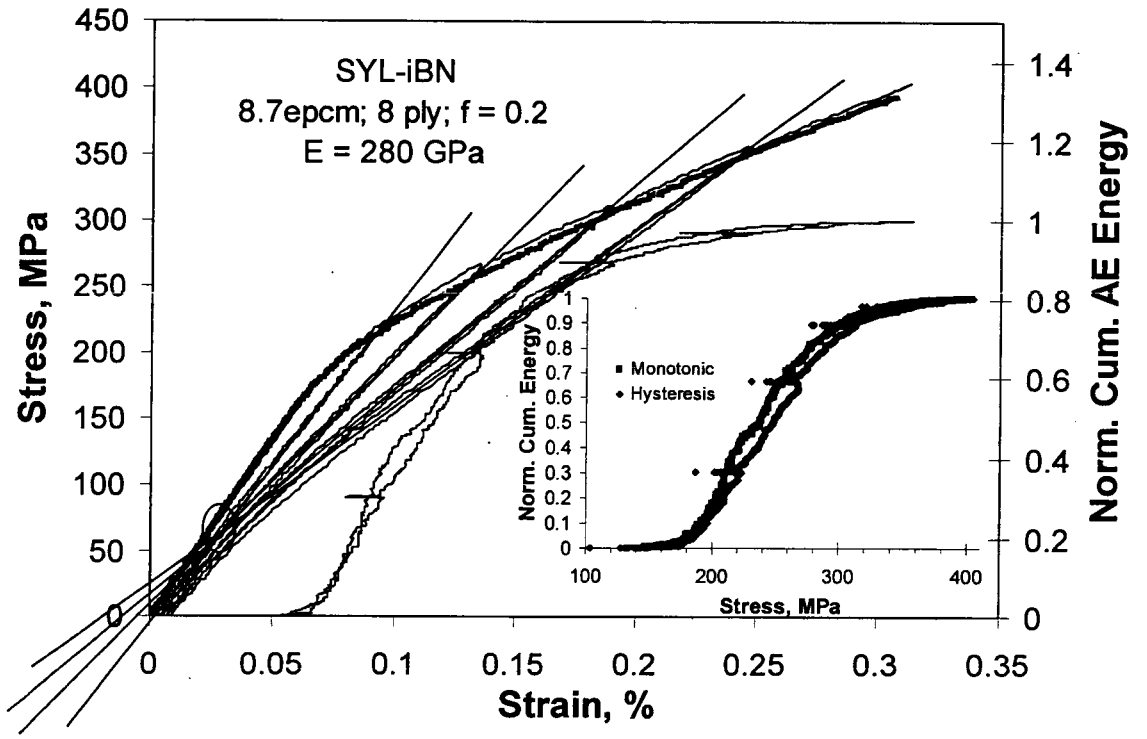

(a)

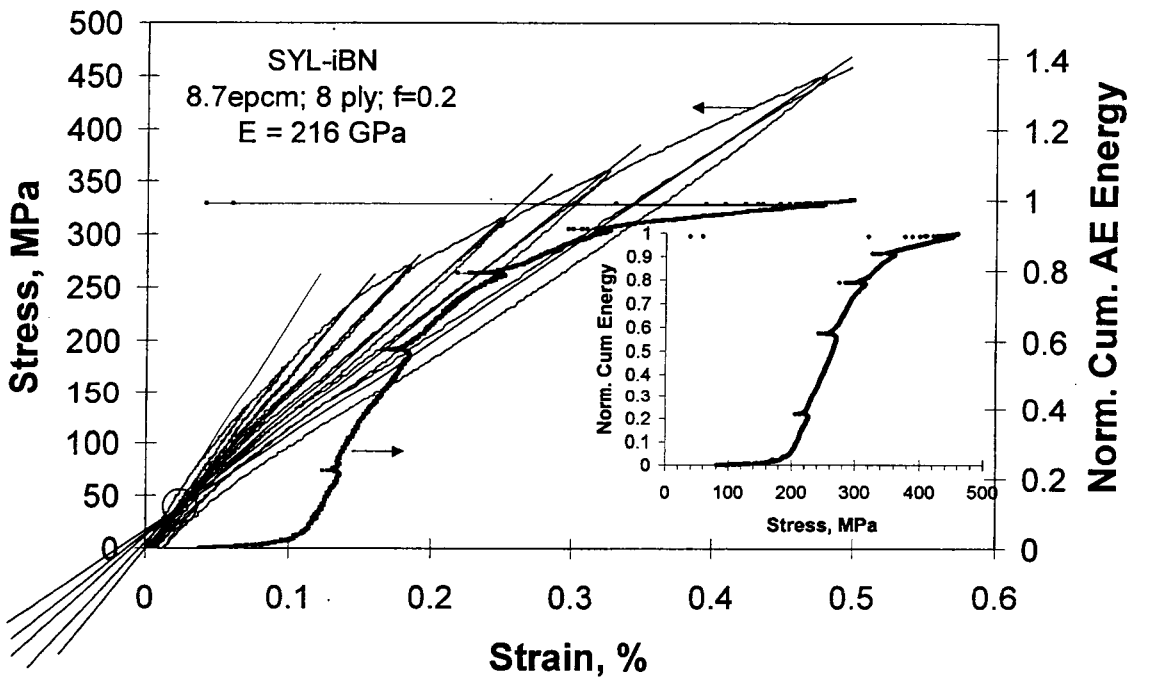

(b)

Figure 2: Tensile monotonic (a) and load-unload-reload hysteresis (a and b) curves for SYL-iBN SiC/SiC composite showing (a) inside debonding and (b) outside debonding. Also plotted is the normalized cumulative AE energy. The AE data is also plotted versus stress in the inset of each plot.

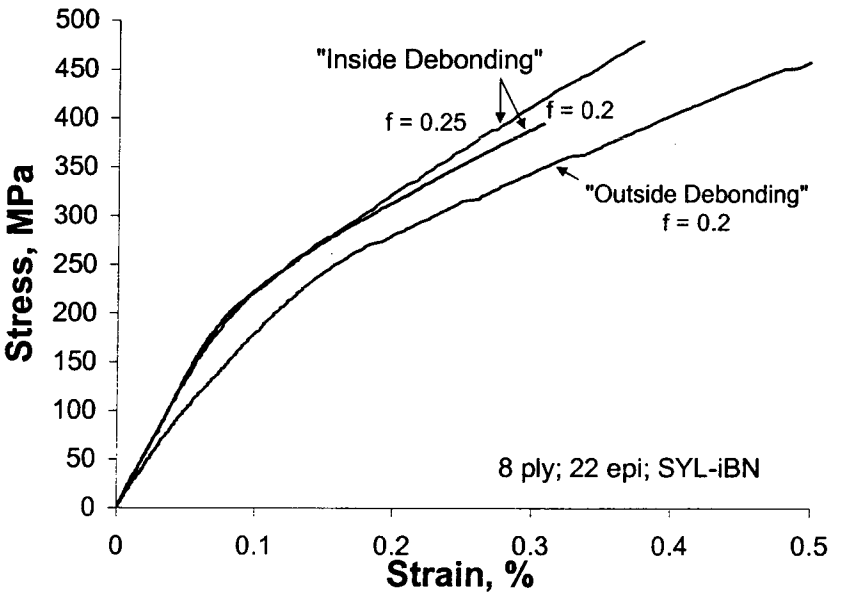

(a)

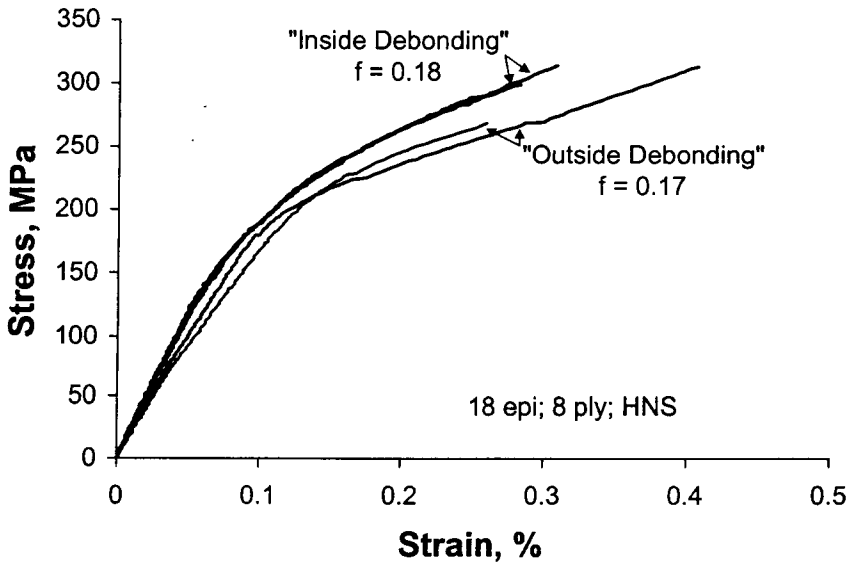

(b)

Figure 3: Room temperature tensile stress-strain curves for (a) 8.7 epcm SYL-iBN SiC/SiC composites and (b) 7.1 epcm HNS SiC/SiC composites (hysteresis loops removed).

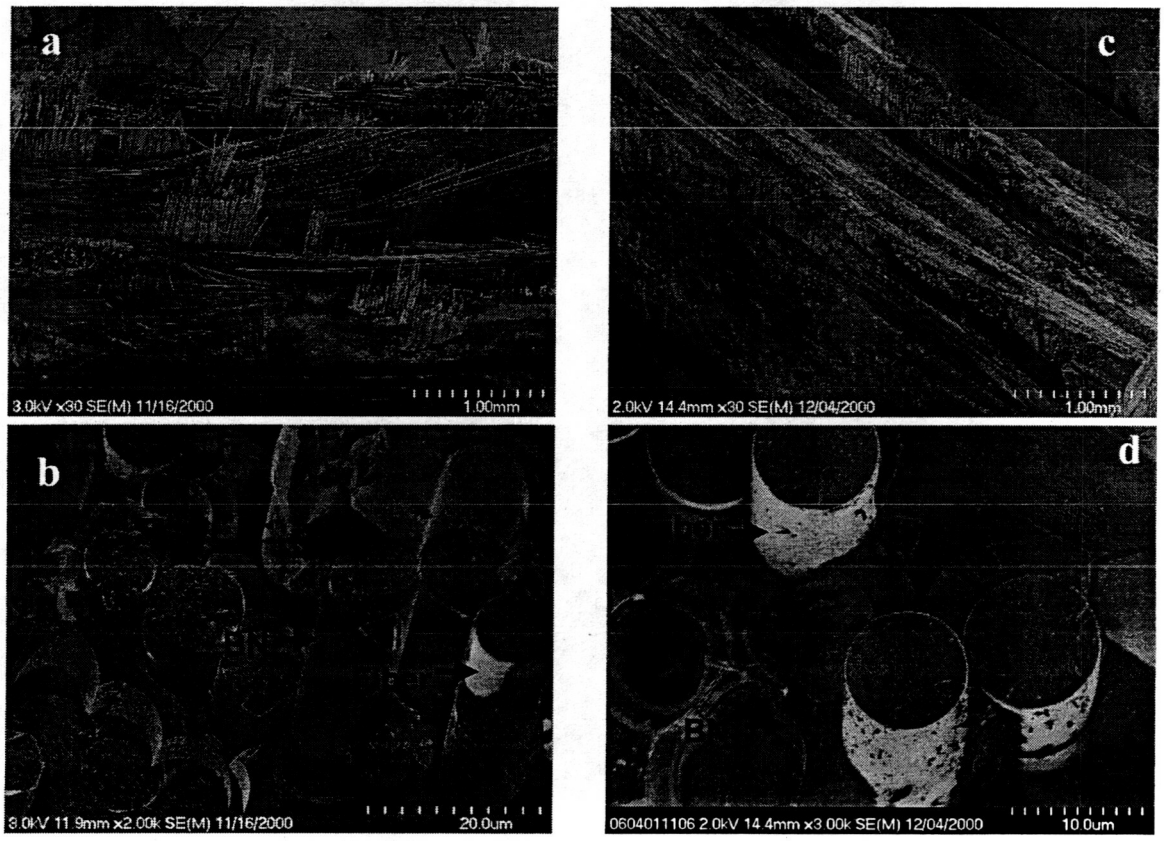

Figure 4: FESEM images of fracture surfaces of SYL-iBN composites showing outside debonding (a,b) and inside debonding (c,d).

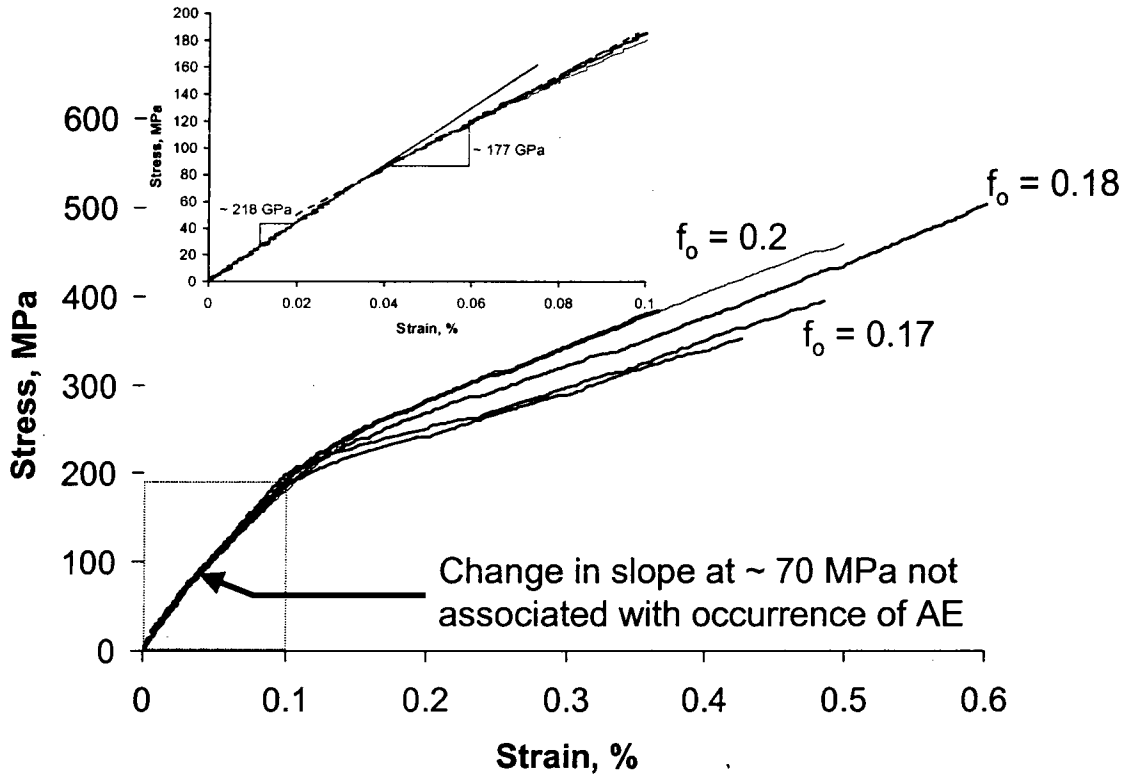

Figure 5: Room temperature tensile stress-strain curves for a number of outside debonding composites with different fiber volume fractions.

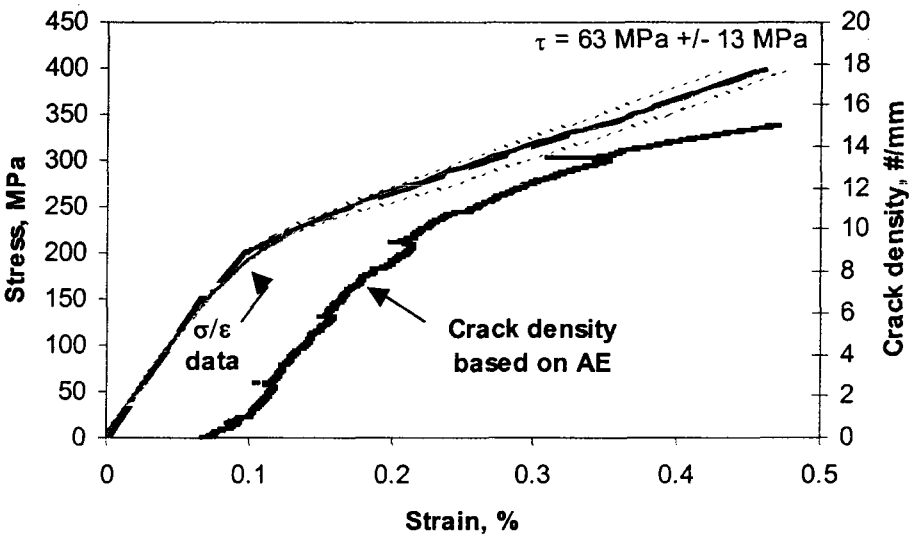

Figure 6: The tensile stress-strain (solid) curve of an inside debonding 5 epcm, 8ply, SYL-iBN, MI composite ($f = 0.12$). The thick dashed line is the best-fit curve for $\tau = 63$ MPa. The thin dashed lines show the predicted stress-strain curves if τ is varied by $\pm$ 20%. The crack density was estimated from AE and the measured final crack density.

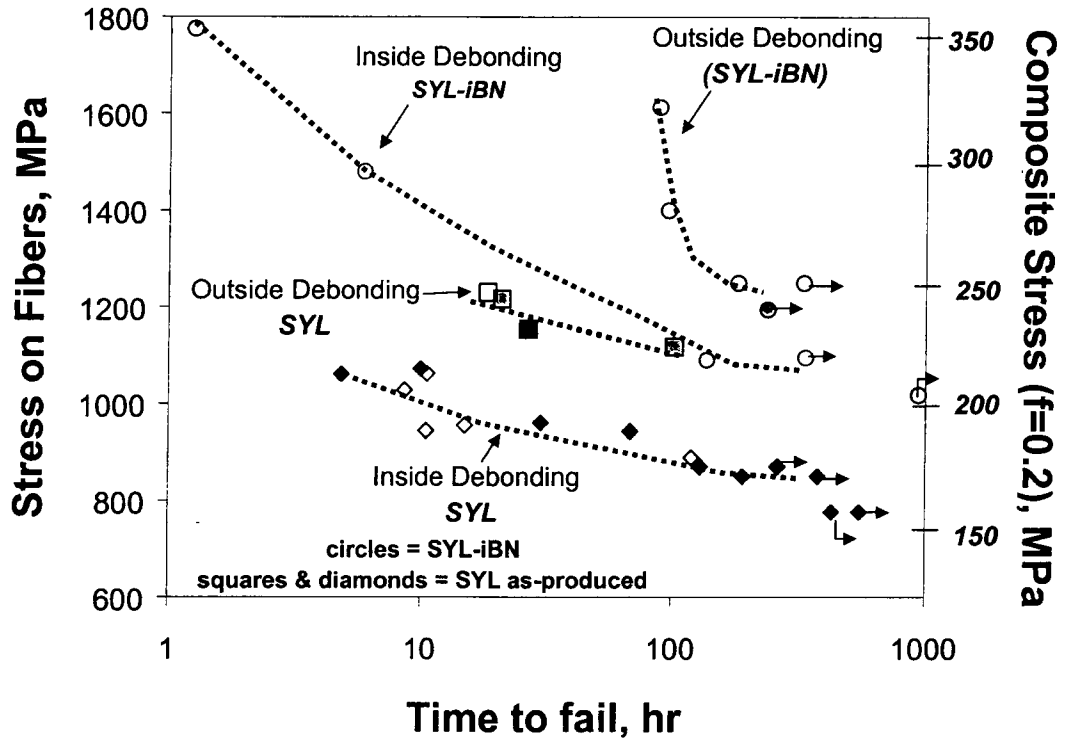

Figure 7: Stress-rupture of inside and outside debonding composites with Sylramic® (SYL) and Sylramic-iBN (SYL-iBN) fiber reinforcement in air at 815°C. The data are plotted as stress on the fibers, i.e., composite stress divided by f. The composite stress for a f = 0.2 is plotted on the right axis.

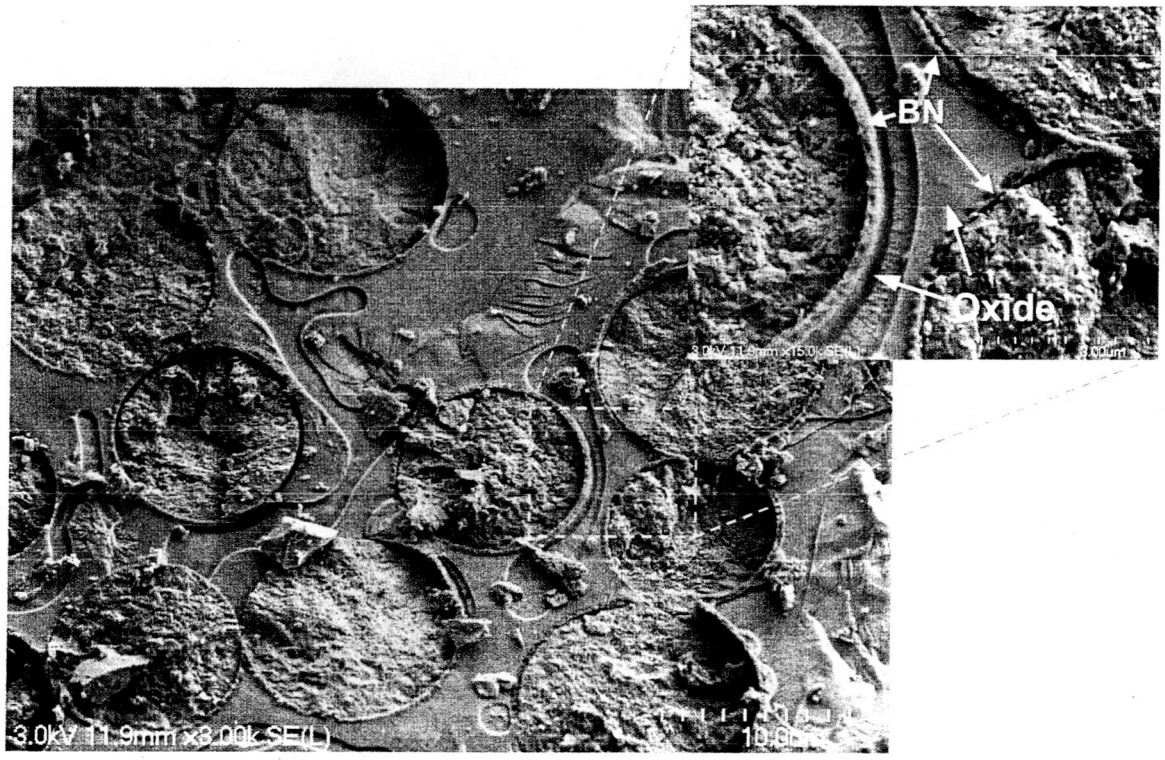

Figure 8: SEM micrograph from the fracture surface of outside debonding composite after stress-rupture after ~ 100 hours at 815°C.

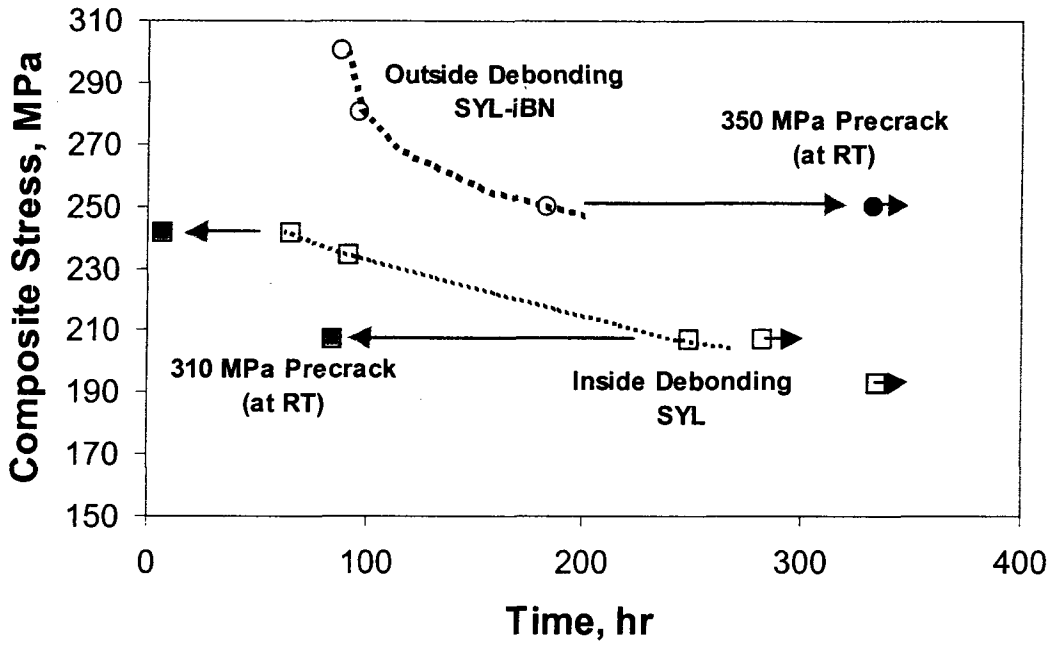

Figure 9: Stress-rupture of as-received and precracked SYL and SYL-iBN SiC/SiC composites at 815°C in air.

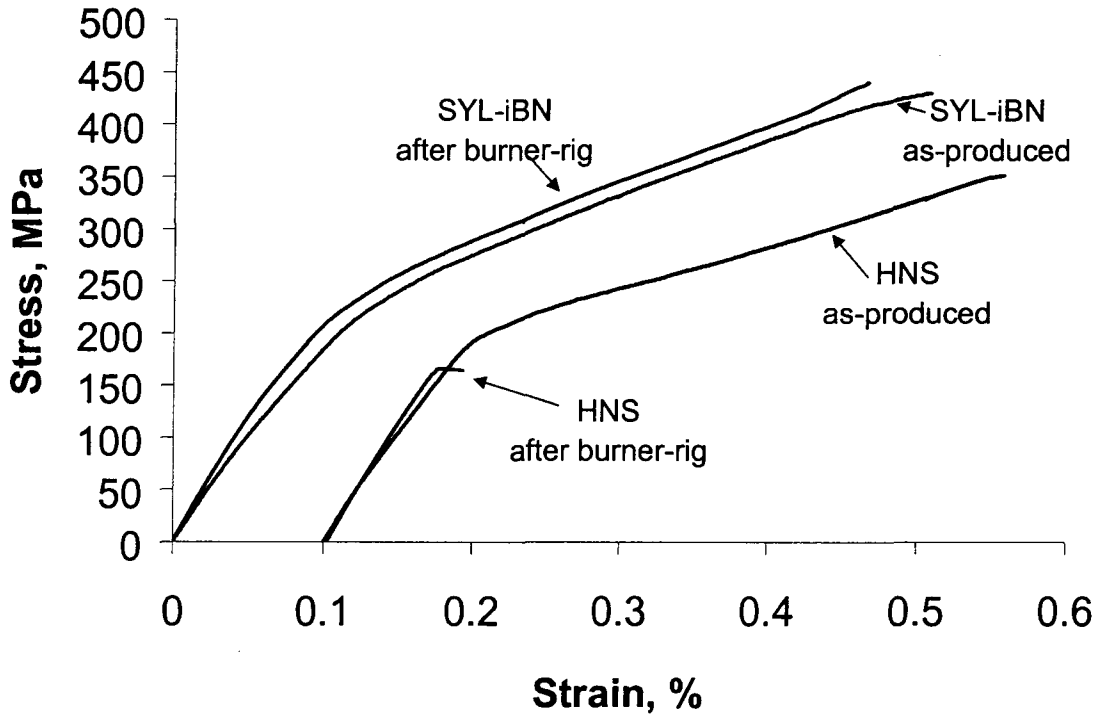

Figure 10: Room temperature tensile stress-strain curves of as-received and burner rig exposed SYL-iBN and HNS SiC/SiC specimens showing outside debonding. The HNS stress-strain curves are offset on the strain axis for clarity.

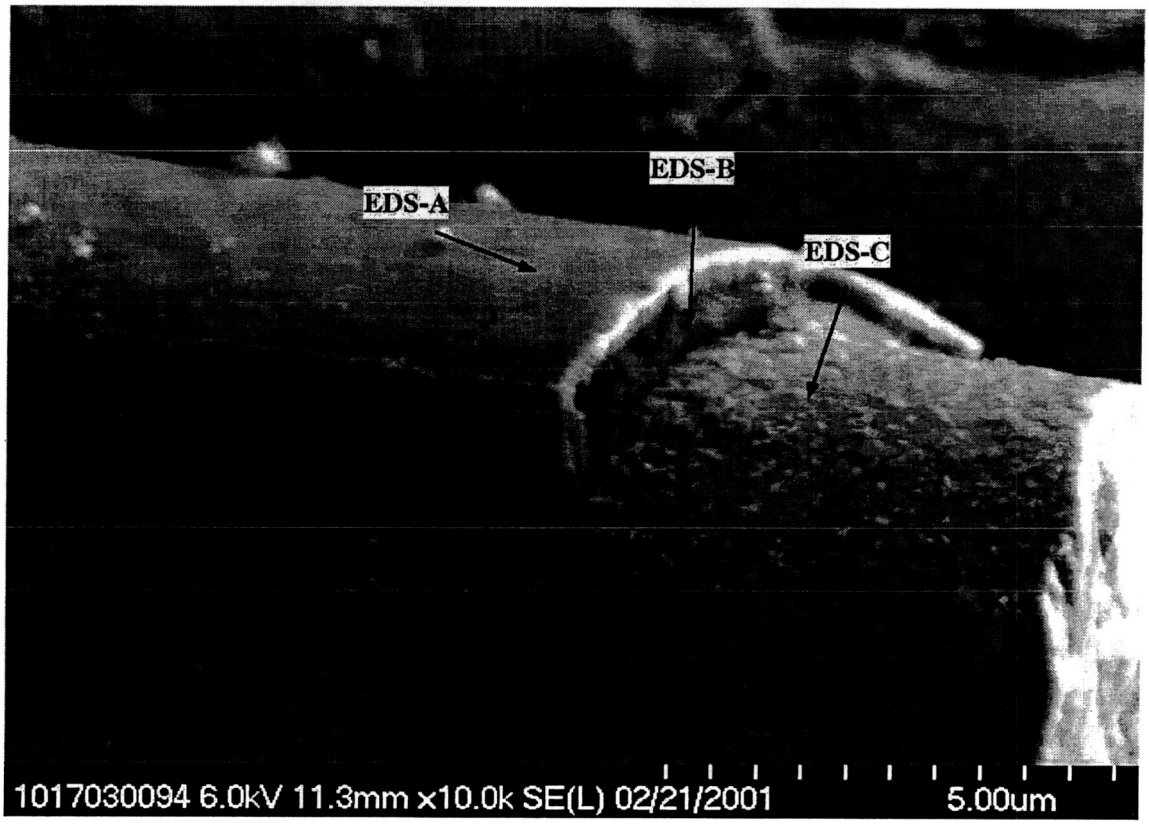

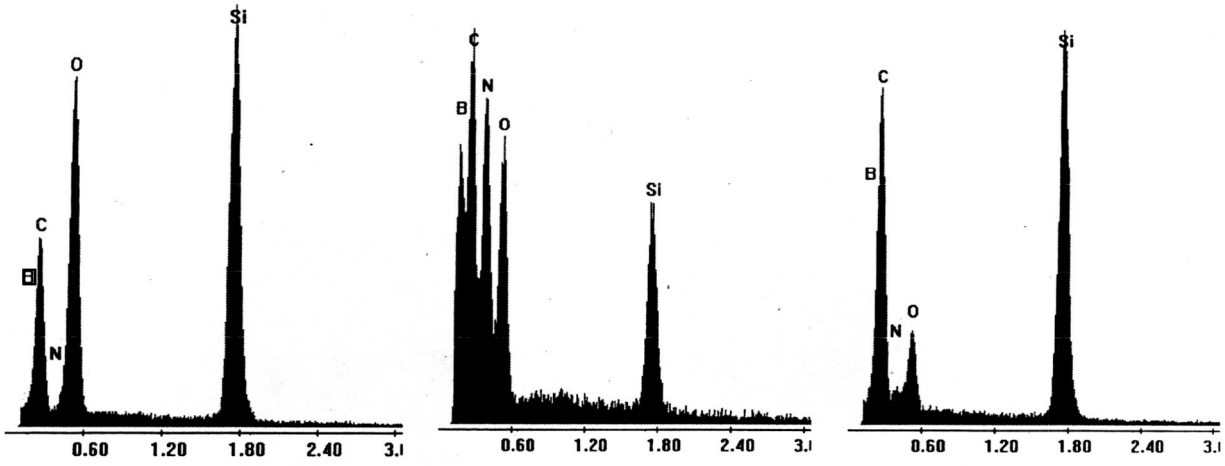

EDS-A: SiO2 EDS-B: BN EDS-C: SiC

Figure 11: SEM micrograph and EDS spectra of regions A, B, and C for outside debonding SYL-iBN SiC/SiC composite after 815°C burner rig exposure and tensile testing at room temperature.

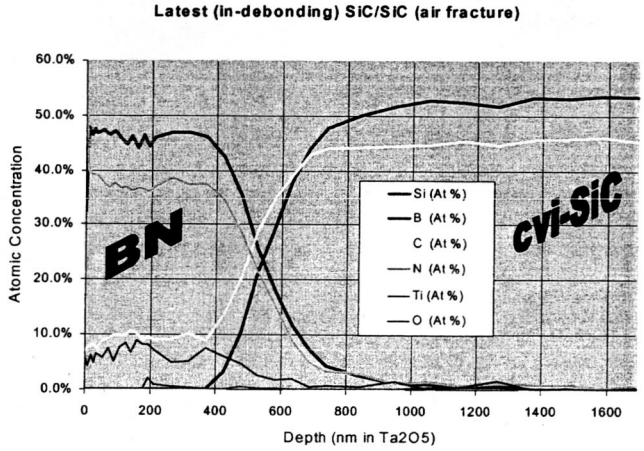

(a)

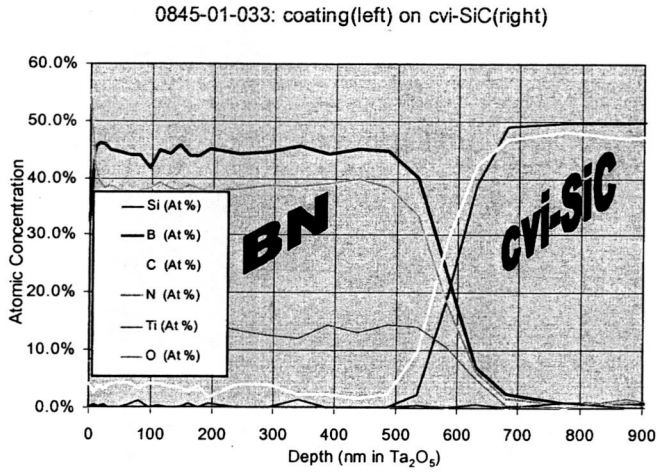

(b)

Figure 12: Typical AES depth profiles of BN layer that adhered to the matrix of SYL-iBN SiC/SiC composites showing (a) inside debonding composite and (b) outside debonding composite.

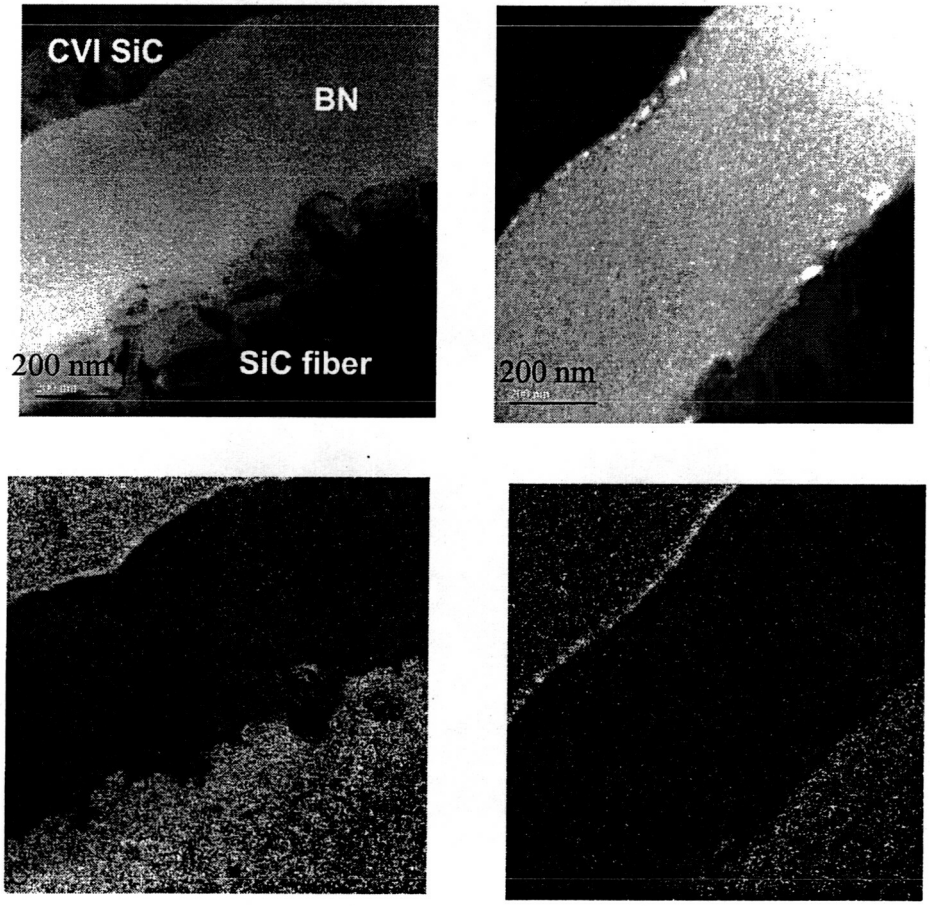

(a) (b)

Figure 13: TEM micrographs (top) and carbon map (bottom, labeled "C") for SYL-iBN SiC/SiC composites showing (a) inside debonding composite and (b) outside debonding composite.